Journal of Advanced Ceramics
2021, **10**(2): 271–278
https://doi.org/10.1007/s40145-020-0437-y
ISSN 2226-4108
CN 10-1154/TQ

Research Article

Fabrication and performance evaluation of novel transparent ceramics RE:$Tb_3Ga_5O_{12}$ (RE = Pr, Tm, Dy) toward magneto-optical application

Xiaoying LI[a,b], Ilya L. SNETKOV[c], Aleksey YAKOVLEV[c], Qiang LIU[d], Xin LIU[a,b], Ziyu LIU[a,b], Penghui CHEN[a,b], Danyang ZHU[a,b], Lexiang WU[a], Zhaoxiang YANG[a], Tengfei XIE[a], Haohong CHEN[a], Oleg PALASHOV[c], Jiang LI[a,b,*]

[a]*Key Laboratory of Transparent Opto-functional Inorganic Materials*, *Shanghai Institute of Ceramics*, *Chinese Academy of Sciences*, *Shanghai 201899*, *China*
[b]*Center of Materials Science and Optoelectronics Engineering*, *University of Chinese Academy of Sciences*, *Beijing 100049*, *China*
[c]*Institute of Applied Physics of the Russian Academy of Sciences*, *Nizhny Novgorod 603950*, *Russia*
[d]*School of Material Science and Engineering*, *Jiangsu University*, *Zhenjiang 212013*, *China*

Received: September 14, 2020; Revised: October 28, 2020; Accepted: November 9, 2020

Abstract: Transparent ceramics are at the heart of modern magneto-optical materials providing promising opportunities for Faraday isolators. 1.0 at% RE:$Tb_3Ga_5O_{12}$ (rare earth (RE) = Pr, Tm, Dy) transparent ceramics were successfully prepared by air sintering and sequential HIP technique using the coprecipitated powders as the raw material. All the powders have shown to be a pure cubic terbium gallium garnet (TGG) phase and exhibit good dispersion. Additionally, a change could not be observed in particle shape with the different doped ions. After the two-step sintering, all the obtained ceramics have good optical quality, and the in-line transmittances at 1070 nm are higher than 80%. Moreover, no secondary phase can be detected from the microstructures. However, the pores which remain entrapped in the ceramics can be noted. The Verdet constant of ceramic samples is optimized by RE doping, and the Verdet constant at 632.8 nm is about –143 rad·T^{-1}·m^{-1}, which is about 5% higher than that of TGG ceramics. Finally, the thermo-optical properties of 1.0 at% RE:TGG transparent ceramics are compared. The annealed TGG ceramic showed the best thermo-optical properties, and the thermally induced depolarization of 1.0 at% Ce:TGG and 1.0 at% Tm:TGG was inferior to that of annealed TGG ceramic.

Keywords: magneto-optical material; rare earth (RE):terbium gallium garnet (TGG) ceramics; Verdet constant; thermo-optical properties

1 Introduction

Optical isolator based on the non-reciprocal Faraday effect is employed widely in laser systems to polarization control [1], isolate [2], and organize the scheme with birefringence compensation [3,4]. The devices can not only allow one-way light transmission, acting as a check valve, but also protect the rest of the system from the back-light [5–7]. Magneto-optical materials

* Corresponding author.
E-mail: lijiang@mail.sic.ac.cn

as the key material of optical isolator own excellent optical quality [8], high Verdet constant [9], good size scalability [10], superior thermal conductivity [11], and high damage threshold [12]. These characterizations are significant when the material is taken into consideration for the application in high-power laser system. Terbium gallium garnet ($Tb_3Ga_5O_{12}$, TGG) single crystals with high transparency in the visible and near infrared regions are employed and they are characterized by high Verdet constant and good thermal conductivity [13–15]. Despite its advantages, the presence of inevitable vaporization of Ga_2O_3 during the growth process may not always be desired as it leads to the formation of color centers, dislocations, or inclusions, thereby degrading the material performance and limiting the crystal size [16,17]. Compared to the corresponding single crystals, TGG transparent ceramics have been fabricated with outstanding optical quality and excellent magneto-optical performances [18–20]. More importantly, they not only maintain excellent optical quality, but also present superior size scalability, allowing an attractive choice for high-power lasers [21–24].

The fast growth of the power in the laser system often results in a large thermal load in magneto-optical element of optical isolators [25,26]. Faraday rotator being the core component of an optical isolator device could play a vital role to miniaturize the overall size of a device in addition to operating at cooling environment [27–30]. Paramagnetic rare earth (RE) ions, mainly Ce^{3+} [31], Pr^{3+} [32], and Nd^{3+} [33] doped TGG crystals have received considerable attention due to their higher Verdet constant than TGG crystals that leads to achieving miniaturization. This is mainly due to the quantum interaction between paramagnetic RE ions and Tb^{3+} ions [34], and the introduction of doping ions changes the crystal field of the matrix material, thus leading to a stronger Faraday effect [35]. It has been demonstrated that Ce^{3+} doping can increase the Verdet constant of TGG transparent ceramics [36]. As is known, Pr^{3+}, Dy^{3+}, and Tm^{3+} also have a large effective magnetic moment, and therefore they are considered as magnetically active ions which can optimize the magneto-optical characteristics of the TGG ceramics. However, as far as we know, the influence of the above RE ions on the optical quality and magneto-optical properties of TGG transparent ceramics, especially the thermo-optical properties, which is significant to the development of new magneto-optical materials, has not been studied yet.

In this work, 1.0 at% RE:TGG (RE = Pr, Tm, Dy) transparent ceramics toward magneto-optical applications were successfully fabricated by a two-step sintering method from high quality nanopowders synthesized by a co-precipitation method. The phase composition and morphology of the calcined powders were studied, and optical quality and microstructure of the corresponding ceramics were systematically investigated. Meanwhile, the influence of RE ions doping on Verdet constant was evaluated. Finally, the thermo-optical properties of 1.0 at% RE:TGG transparent ceramics were compared.

2 Experimental

In the present work, 1.0 at% RE:TGG ceramics were fabricated using the co-precipitated powders as starting material. Detailed experimental procedures for the synthesis of 1.0 at% RE:TGG precursors were presented in our previous work [36]. In a nutshell, the terbium, gallium, and doping ion sources for the 1.0 at% RE:TGG syntheses were all nitrates. Namely, $Tb(NO_3)_3$ (99.99%, Yuelong New Materials Co., Ltd., Shanghai, China), $Ga(NO_3)_3$ (99.995%, Jining Zhongkai New Materials Co., Ltd., Jining, China), and $RE(NO_3)$ were used. The aqueous solutions containing Tb, Ga, and RE nitrates (molar ratio 4.95:3:0.05) were prepared at 0.48 M. The NH_4HCO_3 solution with the concentration of 1.5 M was used as the precipitant and $(NH_4)_2SO_4$ solution as dispersant was added into the precipitant. The precipitant reaction was carried out by the reverse-strike method at the dripping rate of 20 mL/min at room temperature. After aging, in all the cases, the precipitates were washed by centrifugation for several times, first in deionized water and then in absolute ethanol. Finally, the precipitates were dried in an oven at 70 ℃, which were subsequently calcined at 1150 ℃ for 4 h to obtain the 1.0 at% RE:TGG nanopowders. Then the powders were ball-milled in ethanol and 500 ppm GeO_2 was added as sintering additive. Further, the powders were uniaxially dry-pressed into pellets at 40 MPa followed by cold isostatically pressing at 250 MPa. The green bodies were sintered at 1500 ℃ for 3 h in air and successively HIP-ed at 1500 ℃ for 3 h under 150 MPa in Ar atmosphere. Finally, all the doped TGG ceramics were annealed at 1100 ℃ for 5 h. The final 1.0 at% RE:TGG ceramics were mirror-polished on both surfaces to the thickness of 1.5 mm for subsequent characterization.

The powder X-ray diffraction sequence (XRD, D8 Advance, Bruker AXS GMBH, Germany) was recorded for the synthesized RE:TGG nanopowders to analyze the crystallinity and phase compositions in the range of 10°–80° with Cu Kα radiation. The morphology of powders and the microstructure of the thermally-etched surfaces of the 1.0 at% RE:TGG ceramics were submitted to the field emission scanning electron microscopy (FESEM, S-8220, Hitachi, Japan). The average grain size was determined by image analysis from FESEM using the linear intercept method. The specific surface area of the powders was investigated by the nitrogen adsorption method (BET, ASAP 2010, Micrometritics, USA). The in-line transmission spectra of 1.0 at% RE:TGG ceramics were measured in the range of 300–1800 nm using the UV–VIS–NIR spectrophotometer (Cary-5000, Varian, USA). The Verdet constant of 1.0 at% RE:TGG ceramics was measured by using the He–Ne laser with the wavelength of 632.8 nm as source of probe radiation. The applied magnetic field is 1.25 T and the thickness of the samples is 1.5 mm. The test was conducted at room temperature (~25 ℃).

3 Results and discussion

The phase composition of TGG powders doped with different RE ions after calcination was characterized by XRD. The results are shown in Fig. 1(a). The diffraction peaks of all the calcined powders correspond to the TGG standard cards (JCPDS 85-0575), indicating that the calcined powders are pure TGG phase. In addition, the large number of RE^{3+} ions cause distortions in the crystalline structure even if no secondary phases were observed. Figure 1(b) shows the expanded view of the strongest peak in the XRD spectra of 1.0 at% RE:TGG powders compared with the undoped TGG reported in Ref. [18]. It can be seen the shift in diffraction

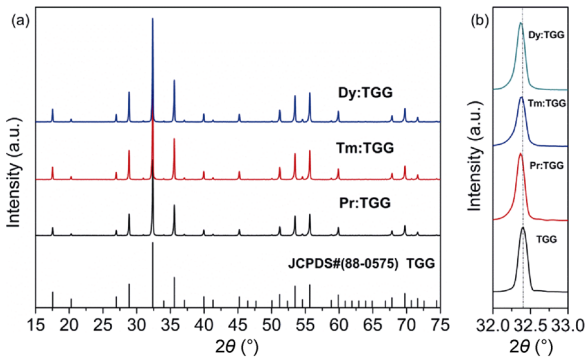

Fig. 1 XRD patterns of (a) 1.0 at% RE:TGG powders calcined at 1150 ℃ for 4 h and (b) the expanded view of the strongest peaks.

peaks of all the calcined powders slightly toward lower angle after being doped with RE ions. The reason for this shift is the case that the ionic radii of the three RE ions are larger than that of Tb^{3+} (92 pm). The ionic radii of Pr^{3+}, Tm^{3+}, and Dy^{3+} are 114, 99, and 103 pm, respectively, and the shift angle changes with the increasing ionic radii of the doping ions.

Figure 2 shows the morphologies of the TGG powders doped with different RE ions. It can be seen that the TGG powders doped with different RE ions have good dispersion and uniform particle size. All powders are composed of peanut-like particles with good crystallinity. The specific surface areas of Pr:TGG, Tm:TGG, and Dy:TGG powders are 4.25, 4.47, and 4.34 m^2/g, respectively. The corresponding average particle sizes are 196.7, 187.0, and 192.6 nm, respectively. The results show that the doped ions have no significant effect on the particle size and dispersion state of 1.0 at% RE:TGG powders.

The 1.0 at% RE:TGG ceramics were annealed at 1100 ℃ for 5 h in air and polished to 1.5 mm thick on both sides, and then the in-line transmittance was tested. Figure 3(a) shows the photograph of different RE ions doped TGG ceramics prepared by air sintering

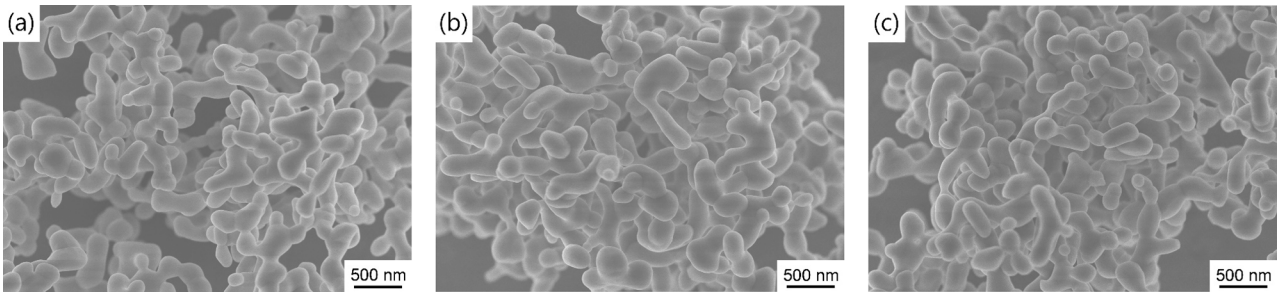

Fig. 2 FESEM images of the 1.0 at% RE:TGG powders calcined at 1150 ℃ for 4 h: (a) Pr:TGG, (b) Tm:TGG, and (c) Dy:TGG.

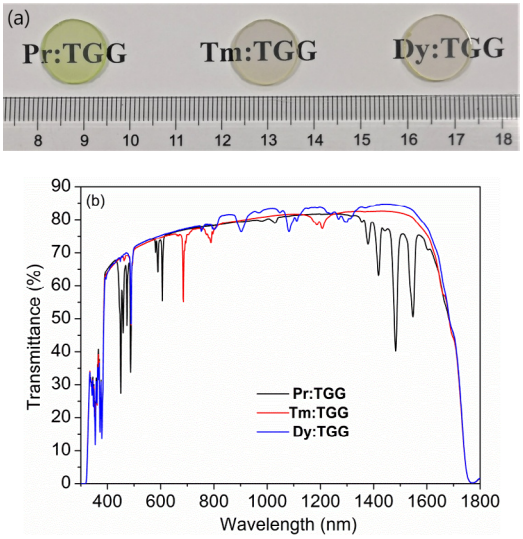

Fig. 3 Photograph and in-line transmission curves of the 1.0 at% RE:TGG ceramics pre-sintered at 1500 ℃ for 3 h in air and HIP-ed at 1500 ℃ for 3 h.

at 1500 ℃ for 3 h and HIP post-treatment at 1500 ℃ for 3 h under 150 MPa. As can be seen, all the RE ions doped TGG ceramics have good optical quality, and the letter at the bottom of the ceramics can be clearly observed. The Pr:TGG ceramics are light green in color; however, the Tm:TGG and Dy:TGG ceramics are colorless, which results from the absorption of RE ions in the visible light band. Figure 3(b) exhibits the in-line transmission curves of the corresponding ceramic samples. It can be seen that the in-line transmittance of Pr:TGG ceramics at 1070 nm reaches 81.0%, and the in-line transmittance at 633 nm is 75.7%. The absorption peaks at 451, 459, and 473 nm correspond to the transitions of Pr^{3+} ions from the ground state $^3H_4$ to excited state $^3P_2$, $^3P_1$+$^1I_6$, and $^3P_0$, respectively. The absorption peaks at 590 and 606 nm are caused by $^3H_4 \rightarrow {}^1D_2$ transition of Pr^{3+} ions. The absorption peaks at 1027 and 1549 nm are due to $^3H_4 \rightarrow {}^1G_4$ and $^3F_3$+$^3F_4$ transitions of the Pr^{3+} ions. The strong absorption peak at 487 nm is ascribed to the Tb^{3+} transition ($^7F_6 \rightarrow {}^5D_4$). The in-line transmittance of Tm:TGG ceramics in the band of 600–1500 nm is higher than 75% (except for the absorption peak), and the in-line transmittance at 1070 nm is 81.5%. According to the transmittance curve, in addition to the absorption peak of Tb^{3+} ions, the absorption peaks at 684, 784, and 1209 nm correspond to the transitions of $^3H_6 \rightarrow {}^3F_{2,3}$, $^3H_4$, and $^3H_5$ of Tm^{3+} ions. The in-line transmittance of Dy:TGG ceramics at 1070 nm is 80.9%, and that at 600 nm is 75.2%. It can be seen that the absorption peaks at 801, 904, 1079, and 1266 nm are attributed to the $^6H_{15/2} \rightarrow {}^6F_{5/2}$, $^6F_{7/2}$, $^6H_{7/2}$+$^6F_{9/2}$, and $^6F_{11/2}$+$^6H_{9/2}$ transitions of Dy^{3+} ions, except for the absorption peak of Tb^{3+} ions. At the same time, the in-line transmittance of all the ceramics decreases in the visible wavelength region, which is mainly related to the existence of sub-micro pores as the scattering centers.

Figure 4 shows the FESEM morphologies of HIP-treated TGG ceramics doped with different RE ions after thermal etching at 1100 ℃ for 1 h in air. The microstructures of the ceramics are quite uniform without abnormal grain growth regardless of doping ions, and no secondary phase is observed at the grain boundaries. The average grain sizes of Pr:TGG, Tm:TGG, and Dy:TGG ceramics are 1.69, 1.73, and 1.77 μm, respectively. All the 1.0 at% RE:TGG ceramics have relatively dense microstructures, and there are only a few nano-pores in the samples, which is the reason for the decline of the in-line transmittance in the visible wavelength region. It is also noted that there are a lot of scratches on the ceramic surface caused by polishing, which will cause optical scattering on the ceramic surface and affect the optical quality of 1.0 at% RE:TGG ceramics. The optical quality of the RE:TGG ceramics can be further improved by optimizing the fabrication process, for instance, to optimize the dispersity and morphology of the raw powders, to

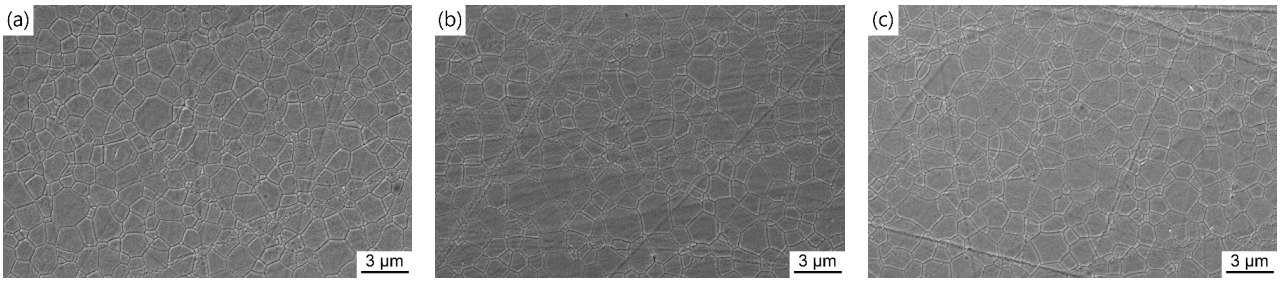

Fig. 4 FESEM micrographs of the 1.0 at% RE:TGG ceramics pre-sintered at 1500 ℃ for 3 h in air and HIP-ed at 1500 ℃ for 3 h: (a) Pr:TGG, (b) Tm:TGG, and (c) Dy:TGG.

optimize the amount of the sintering aid, or to optimize the HIP post-treatment schedules, etc.

The rotation angle of the polarization plane after the light passing the 1.0 at% RE:TGG ceramic element, placed in a fixed magnetic field, was measured at 632.8 nm. The Verdet constant was calculated by the known thickness of the samples, the magnetic field intensity, and the angle of polarization plane rotation. The Verdet constants of Pr:TGG, Tm:TGG, and Dy:TGG ceramics are –142.3, –142.7, and –142.7 rad·T^{-1}·m^{-1}, respectively, which are about 5% higher than that of undoped TGG ceramics. The enhancement of the Verdet constant for the 1.0 at% RE:TGG ceramics is ascribed to the crystal field effect and the quantum interaction between Tb^{3+} and RE ions [20]. The 1.0 at% RE:TGG ceramics exhibit higher Verdet constant, and consequently can contribute to the miniaturization of Faraday isolator device because it will require smaller magnet capacity and shorter magneto-optical element.

Thermally induced depolarization measurement was carried out by the experimental setup shown in Fig. 5. A 1.5 kW Yb:fiber laser manufactured by IPG Photonics operating at a wavelength of 1070 nm with a Gaussian beam profile was employed as the source. Its radiation was used for both heating the studied sample and reading the thermally induced birefringence, which led to the polarization distortions of radiation. Distribution of polarization distortions was registered by CCD camera 6. Calcite wedge polarizer 1 ensured linearity of the polarization and high contrast better than 2×10^{-6} throughout the power range. Fused silica wedges 4 were used to attenuate radiation. Glan prism 5 was adjusted to the minimum power P_d of the laser signal. By rotating the Glan prism by an angle of 90°, we measured the power of the laser signal P_{laser} in the main polarization. The integral thermally induced depolarization $\gamma = P_d/P_{laser}$ was calculated by the ratio of the power in two positions of Glan prism.

For optical ceramics, thermal depolarization can be expressed as [21,37]

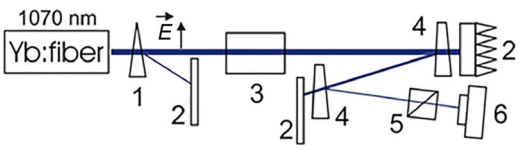

Fig. 5 Scheme of the experiment for the study of thermally induced depolarization: 1-calcite wedge polarizer, 2-absorber, 3-sample, 4-fused quartz wedge, 5-Glan prism, and 6-CCD camera; $\vec{E}$ -electrically induced magnetic field.

$$\gamma = \frac{A}{\pi^2}\left(\frac{2+3\xi}{5}\right)^2 p^2 \quad (1)$$

where ξ is the optical anisotropy parameter, A is the beam shape parameter (A = 0.137 for the Gaussian beam [38]), and p is the normalized power given by the following equation [39]:

$$p = \frac{\alpha_0 Q L P_{laser}}{\lambda k} \quad (2)$$

where L is the sample length, λ is the wavelength, P_{laser} is the laser power, Q is the thermo-optical constant responsible for thermal depolarization, k is the thermal conductivity, and α_0 is absorption coefficient of the ceramic sample. For a TGG crystal, $Q = -17 \times 10^{-7}$ K^{-1} [40], and optical anisotropy parameter ξ is equal to 2.25 [41]. From Eq. (1), it can be seen that the thermally induced depolarization of ceramic sample is directly proportional to the square of P_{laser} and the square of L. Figure 6 shows the γ from the radiation power of undoped TGG ceramics before and after annealing and doped with RE ions: Ce^{3+} [36], Pr^{3+}, Tm^{3+}, and Dy^{3+}. The undoped TGG ceramics were fabricated from co-precipitated nanopowders, and detailed experimental procedures for the synthesis of TGG nanopowders were presented in our previous work [18]. The undoped TGG transparent ceramics were fabricated by air pre-sintering at 1500 ℃ for 3 h followed by HIP post-treatment at 1450 ℃ for 3 h under 150 MPa in Ar atmosphere. The undoped TGG ceramic was annealed at 1100 ℃ for 5 h in air. The in-line transmission curves of the undoped TGG ceramics before and after annealing were presented in Fig. S1 in the Electronic Supplementary Material. All samples have an equal length of 1.3 mm. The line in Fig. 6 represents the analytical approximation of γ calculated by Eq. (1). The TGG ceramic without annealing and Dy:TGG ceramic have the highest level of thermally induced depolarization. The unannealed TGG ceramic sample looks like grayish. This is due to the presence of extra carbon or oxygen vacancies, which significantly increases absorption at 1 μm. Dy^{3+} ions have an absorption peak near 1 μm, which can explain the high level of thermally induced depolarization and this material cannot be used at this wavelength. The annealed TGG ceramic has the lowest level of thermally induced depolarization. When the radiation power is 180 W, the γ is about 5.5×10^{-5}, and then the extinction ratio of TGG ceramic can be calculated to be 42 dB, much higher than the requirements of commercial

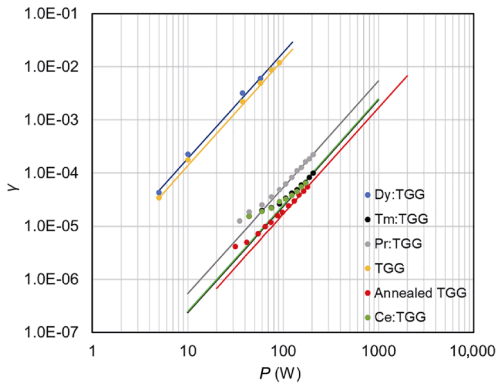

Fig. 6 Experimental (dot) and theoretical (line) dependences of integral thermally induced depolarization on the laser radiation power.

Faraday isolator (> 30 dB). It can be expected that, based on this ceramic material, it is possible to create a Faraday isolator for radiation with a power of ~0.8 kW. The thermally induced depolarization of 1.0 at% Pr:TGG ceramic increases compared to that of the pure TGG ceramic with annealing. Thermally induced depolarization of 1.0 at% Ce:TGG ceramic is comparable to 1.0 at% Tm:TGG ceramic. Moreover, the thermally induced depolarization of 1.0 at% Ce:TGG ceramic and 1.0 at% Tm:TGG ceramic is inferior to that of annealed TGG ceramic. It can be expected that, based on these two ceramic materials, it is possible to create a Faraday isolator for radiation with a power of ~0.65 kW. Compared with pure TGG ceramics, the increasing value of thermally induced depolarization may be caused by the increased absorption due to using a higher dopant concentration and may depend on the ion type. At the same time, the lattice distortion caused by the doping of RE ions decreases the thermal conductivity of RE:TGG ceramics. According to Eq. (1), the decrease of thermal conductivity also leads to the deterioration of the thermo-optical properties of magneto-optical ceramics.

4 Conclusions

In conclusion, starting from nanopowders obtained by the co-precipitate method, transparent 1.0 at% RE:TGG (Pr, Tm, Dy) magneto-optical ceramics with near full density were prepared using a two-step sintering procedure based on the low-temperature sintering process to suppress grain growth without affecting densification. The synthesized 1.0 at% RE:TGG powders were pure phase with similar morphology and good dispersion. All the doped ceramics fabricated by presintering at 1500 ℃ for 3 h in air and HIP post-treating at 1500 ℃ for 3 h showed excellent optical quality, where the in-line transmittance at 1070 nm was higher than 80%. The Verdet constant at 632.8 nm of the doped ceramics was measured to be about –143 rad·T^{-1}·m^{-1}, 5% higher than that of the TGG ceramics, which was beneficial to reduce the size of magneto-optical elements. More importantly, based on the Tm:TGG ceramic, it was possible to create a Faraday isolator for radiation with a power of ~0.65 kW. The annealed TGG ceramic had the best thermo-optical properties with the possibility to create a Faraday isolator for radiation with a power of ~0.8 kW.

Acknowledgements

This work was supported by the National Key R&D Program of China (Grant No. 2017YFB0310500), the NSFC-RFBR Cooperative Research Project (Grant No. 61911530135), and the Key Research Project of the Frontier Science of the Chinese Academy of Sciences (No. QYZDB-SSW-JSC022). This work was supported partially by the Ministry of High Education and Science of the Russian Federation and the State Task executed in the Institute of Applied Physics RAS (Project No. 0035-2019-0015).

Electronic Supplementary Material

Supplementary material is available in the online version of this article at https://doi.org/10.1007/s40145-020-0437-y.

References

[1] Yasuhara R, Furuse H. Thermally induced depolarization in TGG ceramics. *Opt Lett* 2013, **38**: 1751–1753.

[2] Stevens KT, Schlichting W, Foundos G, *et al*. Promising materials for high power laser isolators. *Laser Tech J* 2016, **13**: 18–21.

[3] Yasuhara R, Tokita S, Kawanaka J, *et al*. Cryogenic temperature characteristics of Verdet constant on terbium gallium garnet ceramics. *Opt Express* 2007, **15**: 11255.

[4] Slezak O, Yasuhara Ryo, Lucianetti A, *et al*. Thermally induced depolarization in terbium gallium garnet ceramics rod with natural convection cooling. *J Opt* 2015, **17**: 065610.

[5] Kruk A. Optical and structural properties of arc melted Ce or Pr-doped Y_2O_3 transparent ceramics. *Ceram Int* 2017, **43**: 16909–16914.

[6] Wang XY, Yang L, Chen Z, *et al*. Optical, magnetic susceptibilities and magneto-optical properties of neodymium doped $Tb_3Ga_5O_{12}$ with meliorated properties for near-infrared optical isolators. *J Alloys Compd* 2015, **649**: 1085–1088.

[7] Guo FY, Sun YL, Yang XS, *et al*. Growth, Faraday and inverse Faraday characteristics of $Tb_2Ti_2O_7$ crystal. *Opt Express* 2016, **24**: 5734.

[8] Li XY, Liu Q, Hu ZW, *et al*. Influence of ammonium hydrogen carbonate to metal ions molar ratio on co-precipitated nanopowders for TGG transparent ceramics. *J Inorg Mater* 2019, **34**: 791.

[9] Furuse H, Yasuhara R. Magneto-optical characteristics of holmium oxide (Ho_2O_3) ceramics. *Opt Mater Express* 2017, **7**: 827–833.

[10] Snetkov IL, Yasuhara R, Starobor AV, *et al*. TGG ceramics based Faraday isolator with external compensation of thermally induced depolarization. *Opt Express* 2014, **22**: 4144–4151.

[11] Chen J, Lin H, Hao DM, *et al*. Exaggerated grain growth caused by ZrO_2-doping and its effect on the optical properties of $Tb_3Al_5O_{12}$ ceramics. *Scripta Mater* 2019, **162**: 82–85.

[12] Dai JW, Pan YB, Chen HH, *et al*. Synthesis of Tb_4O_7 nanopowders by the carbonate-precipitation method for $Tb_3Al_5O_{12}$ magneto-optical ceramics. *Opt Mater* 2017, **73**: 706–711.

[13] Li XY, Liu Q, Pan HM, *et al*. Transparent $Tb_3Ga_5O_{12}$ magneto-optical ceramics sintered from co-precipitated nano-powders calcined at different temperatures. *Opt Mater* 2019, **90**: 26–32.

[14] Feng Y, Lin H, Chen C, *et al*. Fabrication of transparent $Tb_3Ga_5O_{12}$ ceramic. *Chin Opt Lett* 2015, **13**: 031602.

[15] Valiev UV, Gruber JB, Burdick GW, *et al*. Optical and magnetooptical properties of terbium–scandium–aluminum and terbium-containing (gallates and aluminates) garnets. *J Lumin* 2016, **176**: 86–94.

[16] Zhuang NF, Song CG, Guo LW, *et al*. Growth of terbium gallium garnet (TGG) magneto-optic crystals by edge-defined film-fed growth method. *J Cryst Growth* 2013, **381**: 27–32.

[17] Chani VI, Yoshikawa A, Machida H, *et al*. Growth of $Tb_3Ga_5O_{12}$ fiber and bulk crystals using micro-pulling-down apparatus. *J Cryst Growth* 2000, **210**: 663–669.

[18] Li XY, Liu Q, Jiang N, *et al*. Fabrication and characterizations of highly transparent $Tb_3Ga_5O_{12}$ magneto-optical ceramics. *Opt Mater* 2019, **88**: 238–243.

[19] Jin WZ, Gai LY, Chen J, *et al*. Fabrication and magneto-optical properties of TGG transparent ceramics. *Phys B: Condens Matter* 2019, **555**: 96–98.

[20] Yasuhara R, Snetkov I, Starobor A, *et al*. Terbium gallium garnet ceramic Faraday rotator for high-power laser application. *Opt Lett* 2014, **39**: 1145–1148.

[21] Yasuhara R, Snetkov I, Starobor A, *et al*. Terbium gallium garnet ceramic-based Faraday isolator with compensation of thermally induced depolarization for high-energy pulsed lasers with kilowatt average power. *Appl Phys Lett* 2014, **105**: 241104.

[22] Yoshida H, Tsubakimoto K, Fujimoto Y, *et al*. Optical properties and Faraday effect of ceramic terbium gallium garnet for a room temperature Faraday rotator. *Opt Express* 2011, **19**: 15181–15187.

[23] Yasuhara R, Nozawa H, Yanagitani T, *et al*. Temperature dependence of thermo-optic effects of single-crystal and ceramic TGG. *Opt Express* 2013, **21**: 31443.

[24] Li J, Dai JW, Pan YB. Research progress on magneto-optical transparent ceramics. *J Inorg Mater* 2018, **33**: 1.

[25] Snetkov IL, Voitovich AV, Palashov OV, *et al*. Review of faraday isolators for kilowatt average power lasers. *IEEE J Quantum Electron* 2014, **50**: 434–443.

[26] Starobor A, Palashov O. The temperature dependence of thermooptical properties of magnetooptical TAG ceramics doped with silicon and titanium. *Opt Mater* 2018, **78**: 15–20.

[27] Yang MQ, Zhou D, Xu JY, *et al*. Fabrication and magneto-optical property of yttria stabilized Tb_2O_3 transparent ceramics. *J Eur Ceram Soc* 2019, **39**: 5005–5009.

[28] Ikesue A, Aung YL, Makikawa S, *et al*. Polycrystalline $(Tb_xY_{1-x})_2O_3$ faraday rotator. *Opt Lett* 2017, **42**: 4399.

[29] Furuse H, Yasuhara R, Hiraga K, *et al*. High Verdet constant of Ti-doped terbium aluminum garnet (TAG) ceramics. *Opt Mater Express* 2016, **6**: 191.

[30] Snetkov IL, Permin DA, Balabanov SS, *et al*. Wavelength dependence of Verdet constant of Tb^{3+}:Y_2O_3 ceramics. *Appl Phys Lett* 2016, **108**: 161905.

[31] Chen Z, Hang Y, Wang XY, *et al*. Fabrication and characterization of TGG crystals containing paramagnetic rare-earth ions. *Solid State Commun* 2016, **241**: 38–42.

[32] Chen Z, Yang L, Wang XY, *et al*. Wavelength dependence of Verdet constant of Pr doped terbium gallium garnet crystal. *Opt Mater* 2016, **62**: 475–478.

[33] Wang XY, Yang L, Chen Z, *et al*. Growth and Faraday rotation characteristics of $Tb_{3-x}Nd_xGa_5O_{12}$ single crystal. *Opt Mater* 2015, **47**: 157–160.

[34] Dai JW, Pan YB, Xie TF, *et al*. A novel $(Tb_{0.995}Ho_{0.005})_3Al_5O_{12}$ magneto-optical ceramic with high transparency and Verdet constant. *Scripta Mater* 2018, **150**: 160–163.

[35] Chen Z, Yang L, Hang Y, *et al*. Improving characteristic of Faraday effect based on the Tm^{3+} doped terbium gallium garnet single crystal. *J Alloys Compd* 2016, **661**: 62–65.

[36] Li XY, Liu Q, Liu X, *et al*. Novel $(Tb_{0.99}Ce_{0.01})_3Ga_5O_{12}$ magneto-optical ceramics for Faraday isolators. *Scripta Mater* 2020, **177**: 137–140.

[37] Liu Q, Li XY, Dai JW, *et al*. Fabrication and characterizations of $(Tb_{1-x}Pr_x)_3Al_5O_{12}$ magneto-optical ceramics for Faraday isolators. *Opt Mater* 2018, **84**: 330–334.

[38] Vyatkin AG, Khazanov EA. Thermally induced scattering of radiation in laser ceramics with arbitrary grain size. *J Opt Soc Am B* 2012, **29**: 3307.

[39] Kagan MA, Khazanov EA. Thermally induced birefringence in Faraday devices made from terbium gallium garnet-

polycrystalline ceramics. *Appl Opt* 2004, **43**: 6030–6039.
[40] Khazanov EA. Characteristic features of the operation of different designs of the Faraday isolator for a high average laser-radiation power. *Quantum Electron* 2000, **30**: 147–151.
[41] Khazanov E, Andreev NF, Mal'Shakov A, *et al*. Compensation of thermally induced modal distortions in Faraday isolators. *IEEE J Quantum Electron* 2004, **40**: 1500–1510.